Original Article

One-tenth-activity total-body positron emission tomography versus full-activity imaging in patients with a complex of hepatic malignant tumors: a retrospective study

Guobing Liu[1,2,3,4#], Hui Tan[1,2,3,4#], Xiuli Sui[1,2,3,4#], Chi Qi[1,2,3,4], Yanyan Cao[1,2,3,4], Danjie Cai[1,2,3,4], Pengcheng Hu[1,2,3,4], Yiqiu Zhang[1,2,3,4], Hongcheng Shi[1,2,3,4,5]

[1]Department of Nuclear Medicine, Zhongshan Hospital, Fudan University, Shanghai, China; [2]Institute of Nuclear Medicine, Fudan University, Shanghai, China; [3]Shanghai Institute of Medical Imaging, Shanghai, China; [4]Cancer Prevention and Treatment Center, Zhongshan Hospital, Fudan University, Shanghai, China; [5]Collaborative Innovation Center for Molecular Imaging Precision Medicine, Shanxi Medical University, Taiyuan, China

Contributions: (I) Conception and design: G Liu, H Tan, H Shi; (II) Administrative support: G Liu, H Tan, X Sui; (III) Provision of study materials or patients: P Hu, Y Zhang, H Shi; (IV) Collection and assembly of data: X Sui, C Qi, Y Cao, D Cai; (V) Data analysis and interpretation: G Liu, H Tan, X Sui, C Qi; (VI) Manuscript writing: All authors; (VII) Final approval of manuscript: All authors.

[#]These authors contributed equally to this work as co-first authors.

Correspondence to: Hongcheng Shi, MD, PhD. Department of Nuclear Medicine, Zhongshan Hospital, Fudan University, No. 180 Fenglin Road, Shanghai 200032, China; Institute of Nuclear Medicine, Fudan University, Shanghai, China; Shanghai Institute of Medical Imaging, Shanghai, China; Cancer Prevention and Treatment Center, Zhongshan Hospital, Fudan University, Shanghai, China; Collaborative Innovation Center for Molecular Imaging Precision Medicine, Shanxi Medical University, Taiyuan, China. Email: shi.hongcheng@zs-hospital.sh.cn.

Background: The value of ultra-low-activity 2-[^{18}F]-fluoro-2-deoxy-D-glucose (^{18}F-FDG) positron emission tomography (PET) imaging in patients with hepatic malignancies remains unclear.

Methods: A cross-sectional study was conducted from April 2019 to May 2021 in Zhongshan Hospital, Fudan University. A total of 49 patients with hepatic malignancies, including hepatocellular carcinoma (HCC) (n=13) or intrahepatic cholangiocarcinoma (ICC) (n=36), underwent 60-min dynamic PET imaging, with 15 undergoing full-activity ^{18}F-FDG and 34 undergoing ultra-low-activity ^{18}F-FDG. The kinetic metrics (K_1–k_3, and *Ki*) of tumors were calculated and compared between the activity groups. Another 54 patients (27 each group) with hepatic malignancies, including HCC (n=9), ICC (n=34), and metastases (n=11), underwent static imaging. Image qualities were compared between the groups in terms of 5-point Likert scores (with a score ≥3 fulfilling the clinical requirement), the mean standardized uptake value (SUV_{mean}), the standard deviation of standardized uptake value (SUV_{SD}), and the signal-to-noise ratio (SNR) of the liver; the SUV_{mean} of blood pool and muscle; and the tumor-to-liver ratio (TLR), tumor-to-blood ratio (TBR), and tumor-to-muscle ratio (TMR) of lesions. Intergroup comparisons were performed using Chi-squared test for categorical variables and the Student's *t*-test or the Mann-Whitney test for continuous variables depending on the normality of variables.

Results: There was a nonsignificant difference in the kinetic metrics (K_1–k_3 and *Ki*) of tumors between the activity groups. In static imaging, 1-min full-activity (F_1) and 8-min ultra-low-activity (L_8) images obtained image-quality scores >3 and were thus selected for intergroup comparisons. Nonsignificant differences in SUV_{mean} of liver, blood pool, and muscle were identified between F_1 and L_8 images (P=0.641, P=0.542, and P=0.073, respectively) although the liver SNR was slightly higher in F_1 (13.10 *vs.* 11.31; P=0.003). Lesion detectability was 98.5% and 100% for F_1 and L_8 images, respectively, but there were no significant differences in TLR, TBR, or TMR between the groups.

Conclusions: The results of this single-center study indicate that the performance of ultra-low-activity

PET imaging is comparable to that of full-activity imaging in patients with hepatic malignancies.

Keywords: Ultra-low-activity; total-body imaging; positron emission tomography/computed tomography (PET/CT); hepatic malignancies; dynamic imaging

Submitted May 22, 2023. Accepted for publication Sep 22, 2023. Published online Oct 19, 2023.
doi: 10.21037/qims-23-719
View this article at: https://dx.doi.org/10.21037/qims-23-719

Introduction

Positron emission tomography/computed tomography (PET/CT) with 2-[^{18}F]-fluoro-2-deoxy-D-glucose (^{18}F-FDG) has become a key tool in oncological imaging (1). However, the axial field of view (AFOV) of conventional PET scanners is narrow (15–30 cm), offering low photon-detecting efficiency (2-4). Therefore, for oncological examinations, the European guidelines recommend a dose of at least 3.5 MBq/body weight (kg) as the least acceptable activity for an imaging protocol of 2 min/bed and a PET bed overlap of >30% (5). This means that PET/CT is not suitable for patients who are vulnerable to radiation exposure, such as pediatric patients (6-8). Techniques that do not use ionizing radiation (such as sonography or magnetic resonance imaging) are commonly the first choice for these patients, with PET/CT often being preferred as a complementary imaging tool to conventional scanning.

The recently released uEXPLORER total-body PET/CT system (United Imaging Healthcare, Shanghai, China), with an AFOV of 194 cm, has ushered in a new era of total-body PET (9). This advance affords a >6-fold increase in signal-to-noise ratio (SNR) and an overall >40-fold gain in sensitivity of PET (6,10,11), allowing for PET imaging with low activity of tracer for vulnerable patients (e.g., pediatric patients) (7). In addition, reducing the tracer activity allows for more PET/CT scans to be completed in a single day with a fixed amount of tracer and thus could alleviate the burden of radiopharmaceutical production, given the increasing number of patients who register for PET/CT examination each day.

A considerable amount of effort has been invested in developing methods than can reduce tracer activity in PET imaging, and favorable results have been obtained through reconstructing low-count PET from full-activity imaging (12-19), supporting the feasibility of low-activity PET. In a previous study, we demonstrated a comparable performance between dynamic PET imaging using a 10× reduction of administrated activity and full-activity imaging in acquiring ^{18}F-FDG kinetic metrics in healthy volunteers (20). Furthermore, static total-body PET using half activity was reported to provide a performance equal to that of full-activity conventional PET in patients with lung cancer (21). Based on these findings, we can speculate upon the possibility of using ultra-low-activity (10× reduction) PET for tumor imaging. As the main organ involved in glycometabolism, the liver is commonly used as the reference organ for assessing the metabolism of diseases (22), and hepatic malignancies and metastases develop frequently. Therefore, this study aimed to evaluate the feasibility of using ultra-low-activity imaging in liver malignancies and thus determine whether this protocol can be applied clinically. We present this article in accordance with the STROBE reporting checklist (available at https://qims.amegroups.com/article/view/10.21037/qims-23-719/rc).

Methods

This retrospective cross-sectional observational study was approved by the Institutional Review Board of Zhongshan Hospital of Fudan University (approval No. B2019-160R) and was conducted in accordance with the Declaration of Helsinki (as revised in 2013). Written informed consent was obtained from all participants.

Patient enrollment for dynamic study

The participants in this study were retrospectively selected from another study conducted by our team, in which 180 patients were enrolled from April 2019 to May 2021, in order to investigate the performance of total-body parametric imaging for tumor diagnosis through dynamic PET imaging, including full-activity and ultra-low-activity imaging, which were evenly and randomly arranged. However, the kinetic metrics used for analyses in this study have not been previously investigated or published. A total of 49 patients with pathologically confirmed hepatic cancers were enrolled to this study (*Figure 1A*); their basic

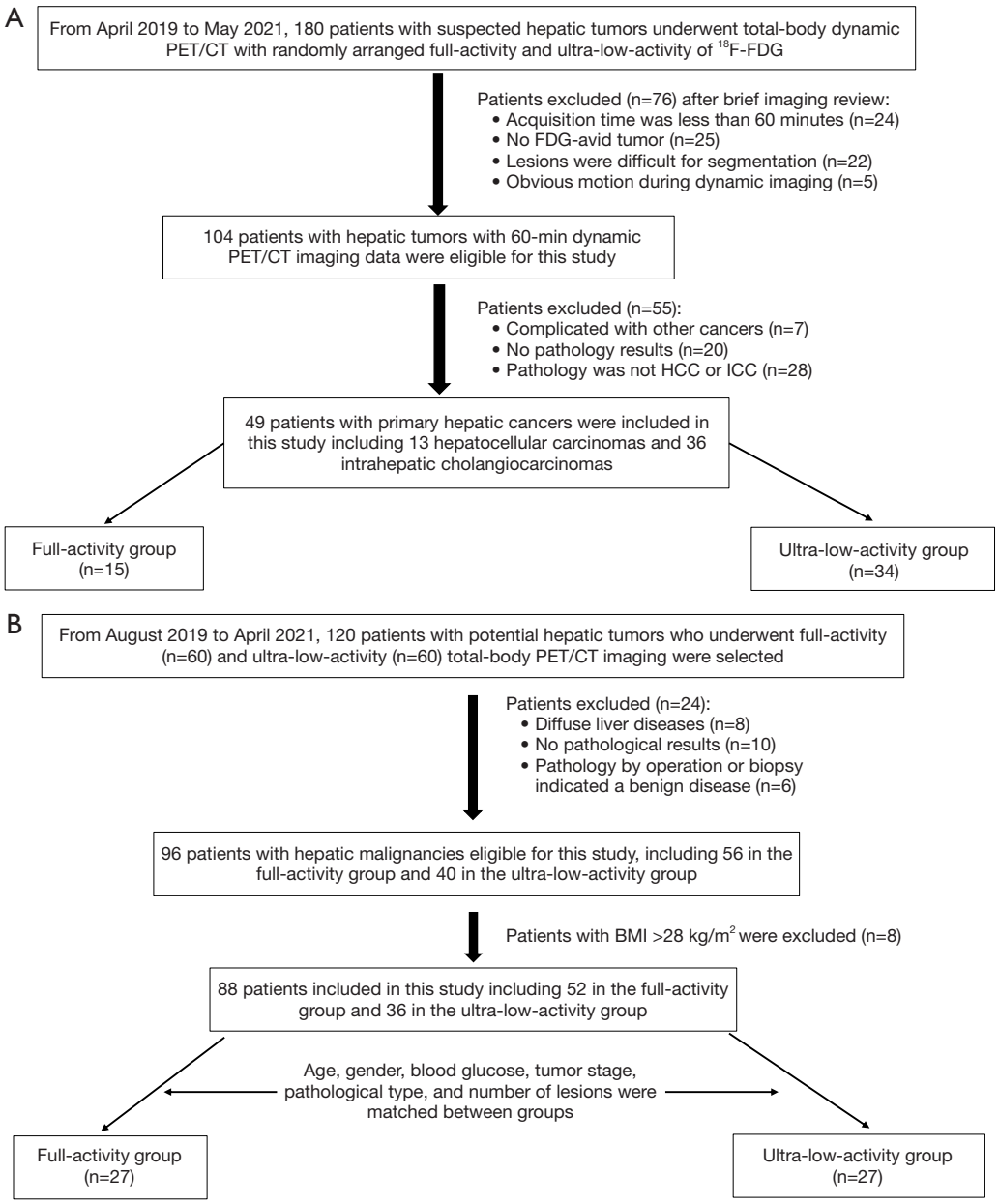

Figure 1 The enrollment flowchart of this study. (A) Dynamic imaging study. (B) Static imaging study. PET/CT, position emission tomography/computed tomography; BMI, body mass index; ^{18}F-FDG, 2-[^{18}F]-fluoro-2-deoxy-D-glucose; HCC, hepatocellular carcinoma; ICC, intrahepatic cholangiocarcinoma.

information is summarized in *Table 1*. The inclusion criteria included a recent hepatic tumor as indicated by radiological examination. The exclusion criteria were as follows: a history of other cancer, a non-FDG-avid tumor, multiple lesions that were difficult to segment, acquisition time of dynamic PET less than 60 min, obvious motion during dynamic PET imaging, no pathological results, and a postoperative tumor pathology that was not hepatocellular carcinoma (HCC) or intrahepatic cholangiocarcinoma (ICC).

Patient enrollment for static study

A total of 120 patients with suspected hepatic malignancies were enrolled for static total-body PET/CT imaging from

Table 1 Basic information of the 49 patients included for dynamic imaging

Variables	Group		P value
	Ultra-low-activity (n=34)	Full-activity (n=15)	
Sex			0.940†
Male	20	9	
Female	14	6	
Age (years)	57 [43–72]	63 [44–81]	0.321‡
Height (cm)	164.30±8.68	166.88±8.30	0.336§
Weight (kg)	61.81±8.77	62.67±11.28	0.776§
BMI (kg/m^2)	22.86±2.41	22.49±3.79	0.677§
Blood glucose (mmol/L)	5.68±0.96	5.72±1.28	0.672§
Injection activity (MBq)	24.79 [17.72–33.37]	218.95 [185.26–323.01]	<0.001‡
Pathology type, n			0.286†
HCC	7	6	
ICC	27	9	

Data are presented as number, median [range] or mean ± SD. †, Chi-squared test; ‡, Mann-Whitney test; §, Student's *t*-test. BMI, body mass index; HCC, hepatocellular carcinoma; ICC, intrahepatic cholangiocarcinoma; SD, standard deviation.

August 2019 to April 2021, with 60 each arranged for full-activity and ultra-low-activity imaging. Of these patients, 32 were excluded due to (I) diffuse liver disease (n=8); (II) a lack of pathology results (n=10); (III) a benign disease confirmed by postoperative or biopsy pathology (n=6); and (IV) body mass index >28 kg/m^2 (n=8). Consequently, 88 patients were included in this study, with 52 in the full-activity group and 36 in the ultra-low-activity group. Finally, 27 patients in each of these groups were selected for final analysis, with patient age, gender, blood glucose level, tumor stage, pathological type, and number of lesions being matched between groups, as shown in *Figure 1B*.

Dynamic PET imaging

For dynamic PET imaging, 15 patients were injected with ^{18}F-FDG of ~3.7 MBq/kg (full-activity group), while the remaining 34 received a 10× reduced dose (~0.37 MBq/kg; ultra-low-activity group). Immediately after injection, the patients underwent total-body dynamic PET for 60 min with the uEXPLORER scanner. Corrections for attenuation, scatter, randoms, and radioactive decay were applied before the PET data were reconstructed into images with a matrix of 239×239×679 (the voxel size was about 2.85 mm^3). The ordered subsets expectation maximization algorithm (OSEM) incorporating point-spread function modeling (PSF) and the time-of-flight (TOF) technique was used with three iterations, 20 subsets, and a Gaussian postfilter of 3 mm. Subsequently, a CT scan was performed with a modulated tube current and a tube voltage of 120 kV for the body, while for the head, the current and voltage were 258 mAs and 120 kV, respectively. The collimation was set to 64×0.5 mm, the pitch to 1.0, and the matrix dimension to 512×512. The PET data were divided into frames as follows: a frame every 5 s for the initial 3 min and a frame every 3 min thereafter. As shown in *Figure 2*, the time-to-activity curves (TACs) of tumors were extracted using an automatic adaptive isocontour volumes of interest (VOIs) around the lesions (23). Furthermore, VOIs were generated by drawing circular regions of interest (ROIs) in ten consecutive axial images in the descending aorta to obtain the image-derived input function (*Figure 2*).

Model fitting for parameter generation

TAC data were fitted with the PMOD Kinetic modeling tool (version 3.2, PMOD Technologies, Zürich, Switzerland) using the standard 2-tissue compartment model. Detailed information regarding model fitting has been published elsewhere (20,24). The constant rates (including K_1 to k_3) and *Ki* were generated, and the determiner index (R^2) was selected for assessing the goodness of fit.

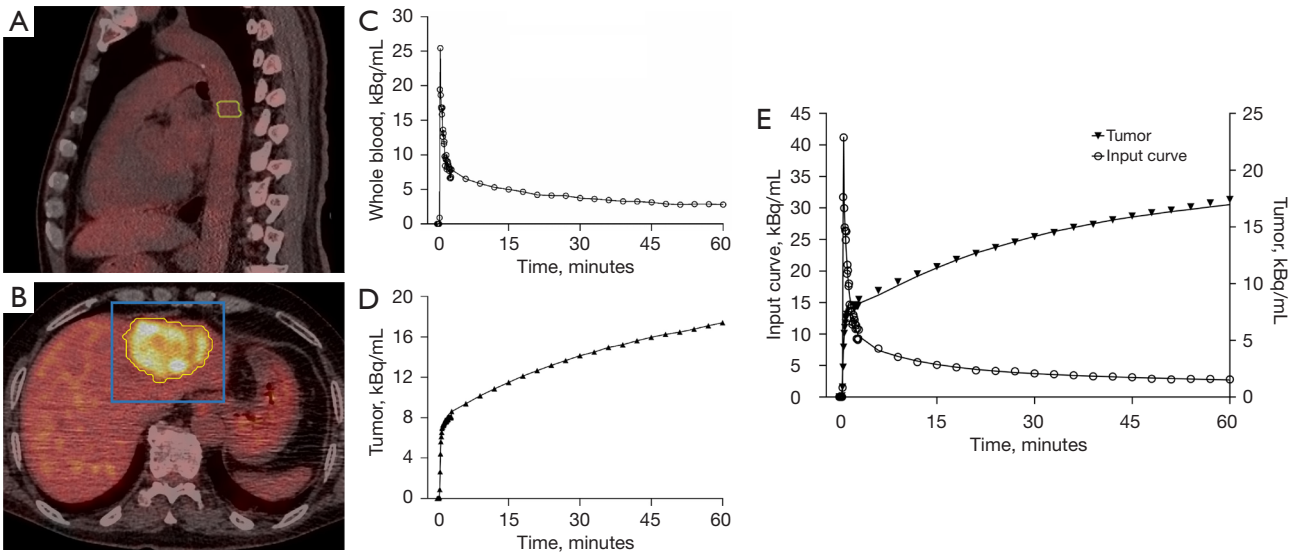

Figure 2 Process of TAC extraction and model fitting. (A) A cylindrical VOI was placed in the descending aorta for generating the whole-blood activity curve, as shown in panel (C). (B) Axial fused PET/CT images showing an ^{18}F-FDG-avid tumor in right lobe of tumor. A rectangle (blue) was drawn to include the whole tumor and an adaptive isocontour VOI (yellow) was automatically generated. Then, TAC of the tumor was extracted from the VOI, as shown in panel (D). Plasma correction was conducted on the curve in panel (C) to generate the image-derived input curve and was uploaded together with the TAC in panel (D) to the PMOD (π modeling) software for kinetic model fitting, as shown in panel (E). TAC, time-to-activity curve; VOI, volume of interest; PET/CT, positron emission tomography/computed tomography; ^{18}F-FDG, 2-[^{18}F]-fluoro-2-deoxy-D-glucose.

Static PET imaging

Static PET was acquired in the 3-dimensional list mode for 15 min after participants had fasted for at least 6 hours and rested for ~1 hour after ^{18}F-FDG injection. The PET images of the full-activity group were divided into the data of the first 0.5, 1, 2, 3, and 5 min, denoted as $F_{0.5}$, F_1, F_2, F_3, and F_5, respectively. The PET images of the ultra-low-activity group were reconstructed with the data of the first 2, 4, 6, 8, 10, and 15 min, defined as L_2, L_4, L_6, L_8, L_{10}, and L_{15}, respectively. PET images were reconstructed into a slice thickness of 1.443 mm and an FOV of 600 mm (voxel size of approximately 2.85 mm^3), using OSEM, TOF, and PSF (OSEM-TOF-PSF) with three iterations, 20 subsets, and a matrix of 192×192.

Subjective analysis of static PET images

First, two nuclear medicine physicians (with 5 and 14 years of experiences, respectively) were trained to retrospectively evaluate the PET images using the 5-point Likert scale (5-PS) method in approximately 70 patients to achieve high interreader consistency (25). Image quality was scored based on three criteria: the overall impression, image noise, and lesion conspicuity. The scores were defined as follows: (I) image with a nondiagnostic quality, unfavorable lesion contrast, or excessive noise; (II) acceptable image quality but with suboptimal noise and lesion depiction; (III) image with quality equal to that used in clinical practice; (IV) image with quality superior to the average image quality; and (V) image with optimal noise, excellent quality, no artifact, and sharp lesion depiction. Typical PET images illustrating the 5-PS scores are shown in *Figure 3*. This 5-point Likert score applies mainly for the use of the uEXPLORER PET/CT scanner but is also suitable for a conventional PET/CT scanner with a state-of-art configuration, for example the uM780 PET/CT scanner (United Imaging Healthcare). Images with a score ≥3 were considered to fulfill the requirement for a clinical diagnosis. The two reviewers evaluated the static PET images of this study independently, and the average score was used for analysis. Three cross-sections of PET images of the chest (at the pulmonary bifurcation level), abdomen (at the portal vein bifurcation level), and pelvis (at the middle level of the third sacral

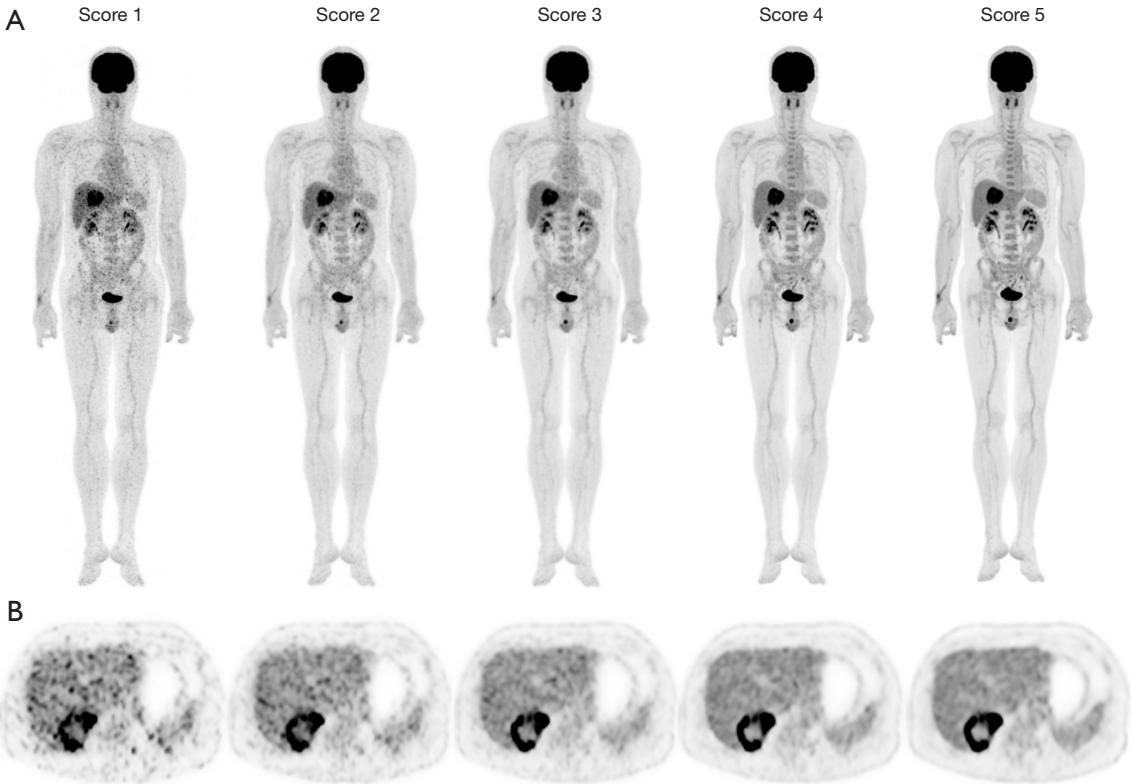

Figure 3 Typical images illustrating the 5-point Likert scales for subjective assessment of static image quality. (A) Maximum intensity projection of PET. (B) Axial images in the section level of the liver. PET, positron emission tomography.

vertebra) were selected for review, with the average score of the cross-sections being used for analysis. The image sets that with the least acquisition time but with an overall 5-PS score ≥3 were selected for comparison between the full-activity and ultra-low-activity groups.

Objective analysis of static PET images

The objective image quality assessment was performed by assessing ^{18}F-FDG uptake in the liver, blood pool, and skeletal muscle. For the liver, four circular ROIs (diameter 2 cm) were placed in the left external lobe and in the upper, middle, and lower area of the right lobe, with visible lesions and large vessels being avoided. For blood pool, an as-large-as-possible ROI was drawn in the ascending aorta (with no wall contact) at level of pulmonary bifurcation. For muscle, ROIs were placed in the gluteus maximus at the middle level of the third sacral vertebra. For each ROI, standardized uptake values, including the mean (SUV_{mean}) and standard deviation (SUV_{SD}) were determined. If multiple ROIs were drawn within a single organ, the average value was obtained for analysis. Furthermore, the liver SNR was calculated by dividing the liver SUV_{mean} by the liver SUV_{SD}. Identical ROIs were copied among the different image sets of each patient.

Objective analysis of lesion demonstration in static PET

According to the PET Response Criteria in Solid Tumors (PERCIST), we defined a positive lesion on PET as follows: SUL_{peak} of lesion >1.5 × SUL_{mean} + 2.0 × SUL_{SD} of the background liver, where SUL denotes SUV normalized by lean body weight (26). The number of lesions was counted, and the lesion detectability was calculated, with F_5 and L_{15} being taken as references for the full-activity and ultra-low-activity groups, respectively. Additionally, the tumor-to-liver ratio (TLR), tumor-to-blood ratio (TBR), and tumor-to-muscle ratio (TMR) were calculated by dividing tumor SUV_{max} by SUV_{mean} of the background liver, blood pool, and muscle, respectively. All lesions were measured if there were fewer than ten lesions; otherwise, the three lesions with the highest ^{18}F-FDG uptake were measured.

Table 2 Basic and clinical information of the patients enrolled in the static imaging study

Characteristics	Group		P value
	Ultra-low-activity (n=27)	Full-activity (n=27)	
Sex			0.163†
Male	19	14	
Female	8	13	
Age (years)	60 [36–78]	59 [33–83]	0.819‡
BMI (kg/m^2)	23.2±2.4	22.8±3.1	0.652§
Blood glucose (mmol/L)	6.1±1.4	5.9±1.3	0.605§
Injected dose (MBq)	24.3±3.5	229.4±40.2	<0.001§
Waiting time (min)	69.4±10.5	71.3±11.1	0.531§
Pathological pattern			0.616‡
ICC	17	17	
HCC	3	6	
Metastatic cancer	7	4	
Group by lesion number			>0.999†
>10	7	7	
≤10	20	20	
Size of lesion analyzed			
Number	61	67	–
Long diameter (cm)	9.0 [3.0–65.3]	2.5 [0.7–13.0]	0.255‡
Short diameter (cm)	6.0 [2.0–10.7]	2.1 [0.7–9.3]	0.795‡

Data are presented as number, median [range] or mean ± SD. †, Chi-squared test; ‡, Mann-Whitney test; §, Student's *t*-test. BMI, body mass index; ICC, intrahepatic cholangiocarcinoma; HCC, hepatocellular carcinoma; SD, standard deviation.

Statistical analysis

Statistical analyses were performed using SPSS 20 (IBM Corp., Armonk, NY, USA), with 2-sided P values <0.05 indicating significance. The weighted kappa test was performed to evaluate the interrater agreement of the subjective image analysis. Comparisons of categorical variables between groups were performed using the Chi-squared test, while comparisons of continuous variables were performed using the Student's *t*-test if they showed normality in the Kolmogorov-Smirnov test; otherwise, the Mann-Whitney test was used.

Results

Basic and clinical information

In the dynamic imaging study, 180 patients were initially considered eligible, and 49 patients were included for analysis after the exclusion criteria were applied. In the static imaging study, 120 patients were initially eligible, and 88 patients were included for analysis after the exclusion criteria were applied. Ultimately, 54 patients were included for analysis after the potential sources of bias were controlled for. The basic information of patients is shown in *Tables 1*,*2*. The enrollment flowchart of the dynamic study and static study are shown in *Figure 1A*,*1B*, respectively. Regarding the 13 HCCs in the dynamic imaging study, eight were grade II and five were grade III. Of the 36 ICCs, seven were grade III, five were grades II–III, 13 were grade II, and 11 were of undetermined grade. In the static imaging study, the nine HCCs were grade III and grade II in five and four patients, respectively. Regarding the 34 ICCs, seven were grade II, six were grades II–III, seven were grade III, and 14 were of undetermined grade. Of the 11 cases with hepatic metastases, seven originated from grade II–III colon adenocarcinomas, three from grade II pancreatic

Table 3 Comparison of kinetic metrics between the ultra-low-activity and full-activity groups

Variables	Ultra-low-activity	Full-activity	P value
All lesions			
Number	37	18	–
Long diameter (cm)	6.3 [2.2–95.8]	9.0 [3.0–65.3]	0.320†
Short diameter (cm)	3.8 [1.0–24.6]	6.0 [2.0–10.7]	0.174†
K_1 (mL/cm^3/min)	0.359±0.123	0.358±0.168	0.982‡
k_2 (min^{-1})	0.651±0.291	0.632±0.235	0.811‡
k_3 (min^{-1})	0.063 [0.010–0.350]	0.065 [0.012–0.203]	0.970†
Ki (mL/cm^3/min)	0.034±0.015	0.031±0.012	0.468‡
R^2	0.973 [0.910–0.995]	0.983 [0.916–0.998]	0.101†
HCC	7	6	–
K_1 (mL/cm^3/min)	0.331±0.070	0.339±0.156	0.836‡
k_2 (min^{-1})	0.542±0.231	0.527±0.169	0.892‡
k_3 (min^{-1})	0.043 [0.010–0.350]	0.052 [0.012–0.203]	0.391†
Ki (mL/cm^3/min)	0.026±0.023	0.030±0.015	0.366‡
R^2	0.951 [0.910–0.997]	0.989 [0.918–0.998]	0.116†
ICC	30	12	–
K_1 (mL/cm^3/min)	0.365±0.130	0.371±0.172	0.858‡
k_2 (min^{-1})	0.672±0.297	0.695±0.241	0.631‡
k_3 (min^{-1})	0.068 [0.026–0.224]	0.065 [0.018–0.163]	0.802†
Ki (mL/cm^3/min)	0.035±0.013	0.031±0.010	0.401‡
R^2	0.976 [0.882–0.999]	0.982 [0.916–0.999]	0.316†

Data are presented as number, median [range] or mean ± SD. †, Mann-Whitney test; ‡, Student's *t*-test. HCC, hepatocellular carcinoma; ICC, intrahepatic cholangiocarcinoma; SD, standard deviation.

ductal adenocarcinomas, and one from grade II duodenal adenocarcinoma. Except for the injection activity, none of the basic and clinical parameters significantly differed between the ultra-low- and full-activity groups.

Comparison of kinetic metrics

In the 49 patients who underwent dynamic imaging, there were 53 lesions found. The ultra-low-activity and full-activity groups showed no significant differences in kinetic metrics, either in whole or in any pathological subtypes of the tumors (*Table 3*). Both the long diameters and short diameters of lesions analyzed were comparable between the groups. All the fitted models showed excellent goodness of fit (R^2>0.95) in both ultra-low-activity and full-activity groups.

Subjective scores of the static PET images

The 5-PS scores markedly increased with an increase of acquisition time (*Table 4*). F_1 and L_8 reached an overall score higher than 3.0 and were thus selected for intergroup comparisons, with typical cases presented in *Figure 4*. The interrater consistency for subjective image assessment was good, with an overall weighted kappa of 0.800 [95% confidence interval (CI): 0.766–0.834] for full-activity images and 0.742 (95% CI: 0.709–0.776) for ultra-low-activity images.

Comparisons of objective assessments of image quality

As shown in *Figure 5*, the background image qualities in terms of SUV_{mean} of the liver, blood pool, and muscle as well

Table 4 Summary statistics regarding the subjective scores of static PET imaging

Section level	Subjective score (mean ± SD)										
	Full-activity group					Ultra-low-activity group					
	$F_{0.5}$	F_1	F_2	F_3	F_5	L_2	L_4	L_6	L_8	L_{10}	L_{15}
Bronchial bifurcation	2.40±0.46	3.32±0.43	4.13±0.32	4.67±0.38	5.00±0.00	1.23±0.31	1.98±0.31	2.75±0.37	3.12±0.43	3.78±0.39	4.20±0.48
Portal vein bifurcation	2.28±0.39	3.15±0.30	3.88±0.31	4.37±0.37	5.00±0.00	1.28±0.39	2.00±0.42	2.68±0.38	3.07±0.34	4.07±0.32	3.98±0.38
Third sacral vertebra	2.52±0.40	3.48±0.40	4.15±0.23	4.83±0.30	5.00±0.00	1.12±0.25	1.82±0.38	2.52±0.38	3.05±0.36	3.58±0.42	4.03±0.35
Overall	2.24±0.34	3.32±0.29	4.06±0.23	4.62±0.25	5.00±0.00	1.21±0.25	1.93±0.28	2.65±0.32	3.08±0.30	3.66±0.32	4.07±0.32

PET, positron emission tomography; SD, standard deviation; F, full-activity; L, ultra-low-activity.

as the SUV_{SD} of the liver were all statistically comparable between F_1 and L_8. However, the SNR of the background liver in F_1 was significantly higher than that in L_8 (13.10±2.28 *vs.* 11.31±2.11; P=0.003).

Comparisons related to lesion demonstration

With F_5 as the reference, F_1 detected 66 lesions and missed only 1 lesion, yielding a lesion detectability of 98.5% (66/67). The case involving the lesion missed by F_1 is presented in *Figure 6*. In ultra-low-activity imaging, 61 lesions were detected with L_{15} as the reference, of which no lesions were missed by L_8, yielding a lesion detectability of 100% (61/61). The sizes of lesions were comparable between the 2 activity groups (*Table 2*). F_1 and L_8 showed no significant difference in TLR (3.99 *vs.* 4.74; P=0.092), TBR (6.06 *vs.* 7.29; P=0.085), or TMR (15.71 *vs.* 17.19; P=0.469), as shown in *Figure* 7.

Discussion

The liver is the main organ of glycometabolism, and this makes ^{18}F-FDG PET/CT diagnoses of hepatic malignancies challenging, as the ^{18}F-FDG metabolism varies both in hepatic tumors and background normal liver tissue. The distribution of ^{18}F-FDG to organs and tumors involves multiple complicated pharmacokinetic processes. The potential influence of activity reduction (especially a 10× reduction) on these processes remains unclear. In this study, we first investigated the performance of ultra-low-activity (10× reduction) PET in a dynamic imaging scenario. The kinetic parameters identified in ultra-low-activity imaging were comparable to those in full-activity imaging. Next, this comparability was validated in static imaging, both through subjective assessments of image quality and by objective quantification of background metabolism, image contrast, lesion detection, and tumor-to-background contrast.

The total-body PET scanner possesses high sensitivity of count detection, allowing for imaging with low tracer activity (7,10), and tracer activity reduction is a reliable method for reducing radiation exposure. In addition, low-activity PET imaging increases the scope of application of PET/CT in radiation-vulnerable patients (such as children). Furthermore, low-activity PET imaging is suitable for multitracer imaging and for monitoring the therapy response of malignancies, which require repeated PET imaging in a short time interval (27). Dose reduction is particularly relevant for patients with hepatic cancer who may not be able to tolerate cancerous radiation effects within their expected life span. Additionally, PET/CT with reduced tracer activity can serve as a flexible alternative protocol when facing an unexpectedly large number of patients, alleviating the burden of radiopharmaceutical production.

Activity reduction is a consistent focus of PET imaging research. However, due to the limited sensitivity of conventional PET scanners, previous studies of this nature have been restricted to reconstructing low-count PET images from full-activity imaging (12-17). Kaplan *et al.* demonstrated that quality-equal PET images estimated by using 10% of counts could be obtained from full-activity imaging (12). However, these methods are time-consuming because of the substantial computational expenses involved in data processing and uniformly require a predefined regularization, which may lead to undesirable oversmoothing or artifacts. In a recent study, static PET

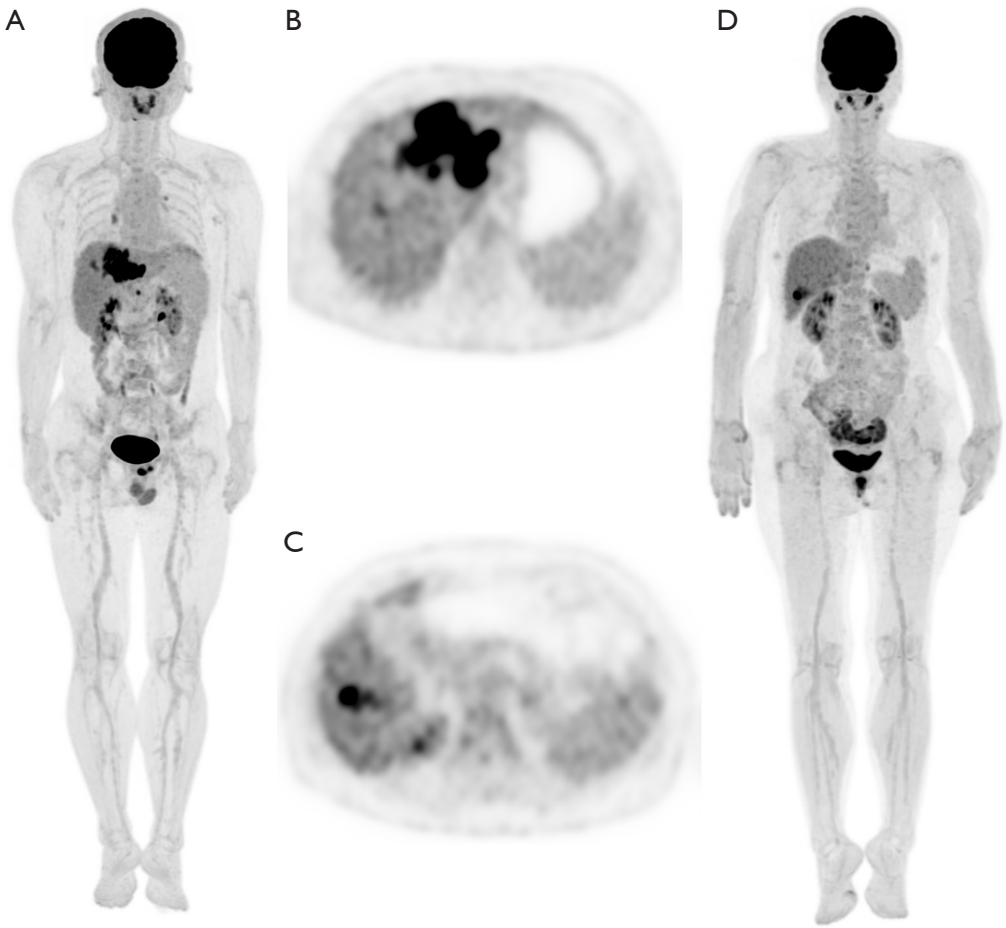

Figure 4 Visual comparison of PET images between F_1 and L_8 from two typical cases. Maximum intensity projection of PET (A,D) and axial images in the section level of the liver (B,C) from typical F_1 (A,B) and L_8 (C,D) image sets illustrating equivalence of image quality, both of which were given a subjective score of 3. Liver SNR was measured as 9.2 for F_1 and as 8.9 for L_8. PET, positron emission tomography; F, full-activity; L, ultra-low-activity; SNR, signal-to-noise ratio.

imaging with a total-body PET scanner involving a real activity reduction to about 15% achieved high image quality (9). Furthermore, in our recent study, an even lower activity of approximately 10% was used in dynamic imaging and demonstrated comparable performance in quantifying the kinetics of ^{18}F-FDG, compared to full-activity dynamic imaging (20). In the present study, for the first time, we validated the performance of PET imaging with 10% activity in patients with hepatic malignancies. An even lower injection activity is possible with the application of deep learning techniques in data reconstruction since a 200× activity reduction has been achieved in PET imaging of the brain (28).

In the static imaging study, we selected the image set with the least acceptable acquisition times for intergroup comparisons. In the full-activity group, the F_1 image reached a quality score of >3, which is consistent of our previous study (29). An even faster imaging protocol of 45 s using the uEXPLORER scanner was also recently reported by our team (30). However, its 5-PS scores (3.19±0.55) were slightly lower than those of F_1 in the current study (3.32±0.29), which might be due to longer acquisition times consistently contributing to a better image quality (31). We did not select the 45-s protocol for full-activity imaging because reduction in acquisition time to 1 min is already remarkable. However, under special conditions in which PET imaging has to be completed as fast as possible, the 45-s protocol may be a viable alternative.

In ultra-low-activity imaging, L_8 also yielded a 5-PS score of >3, indicating a nonlinear gain (10-fold-activity

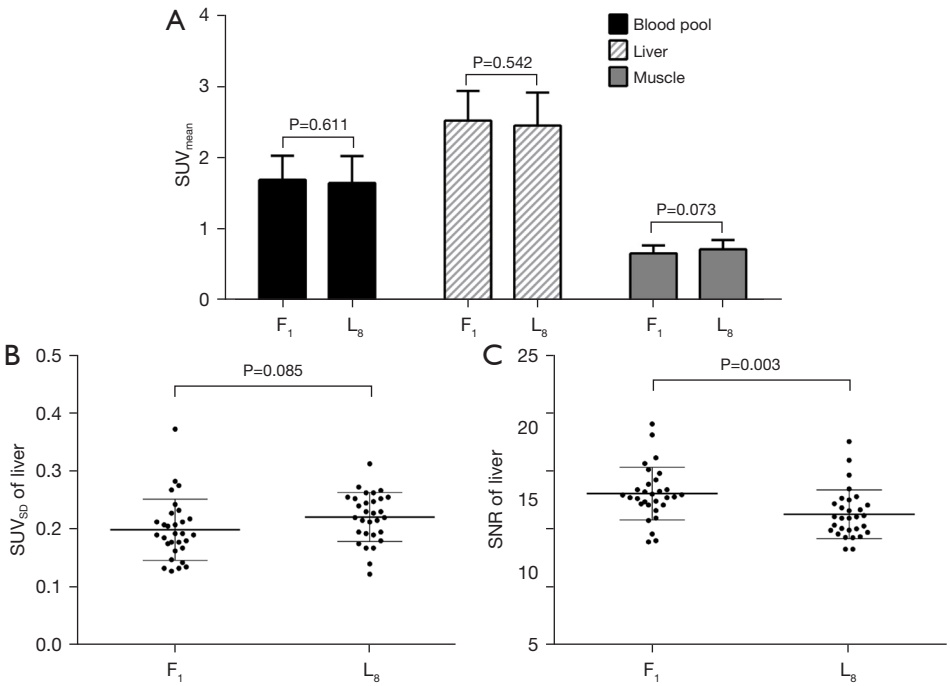

Figure 5 Statistical summary of quantitative metrics regarding background metabolism. Comparisons of background SUV_{mean} (A) in the blood pool, liver, and muscle, as well as the SUV_{SD} (B) and SNR (C) of the liver, between F_1 and L_8. SUV_{mean}, mean standardized uptake value; F, full-activity; L, ultra-low-activity; SD, standard deviation; SNR, signal-to-noise ratio.

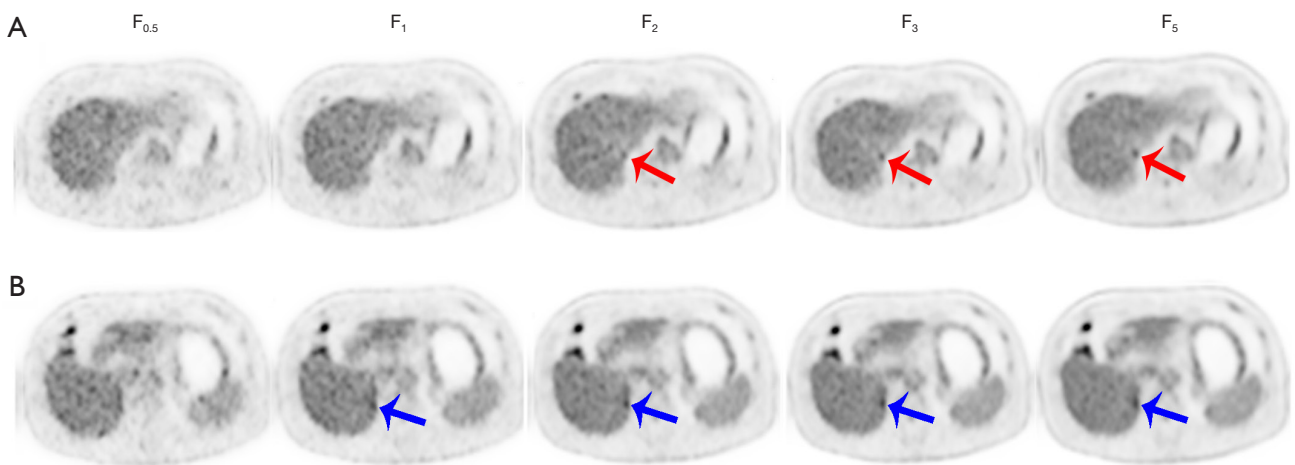

Figure 6 A typical case of a lesion missed by F_1. The patient was a 64-year-old man with 2 lesions that were confirmed to be hepatocellular carcinoma. (A) One lesion (red arrows) could be visualized on F_2, F_3, and F_5 but was not present on $F_{0.5}$ or F_1. (B) Another lesion (blue arrows) could be found on F_1, F_2, F_3, and F_5 but was difficult to visualize on $F_{0.5}$. F, full-activity.

decrease *vs.* a 8-fold-time increase). In addition, the lesion detectability (100% *vs.* 98.5%) and the tumor-to-background contrast (in terms of TLR, TBR, and TMR) were slightly higher in L_8 than in F_1, although none reached statistical significance. These results might be associated with the accessory corrections (TOF and PSF) incorporated in image reconstruction. This is in addition to the obvious FOV-conditioned sensitivity gain which

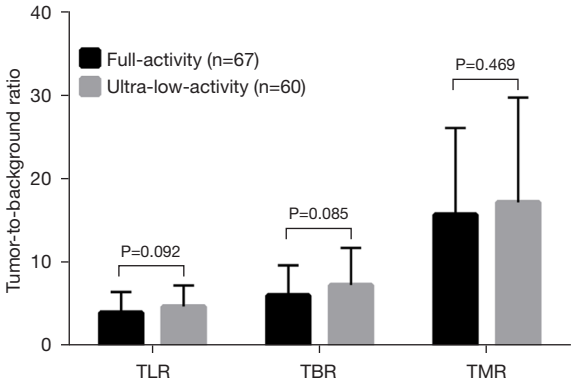

Figure 7 Comparison of the TLR, TBR, and TMR between the full-activity and ultra-low-activity groups. TLR, tumor-to-liver ratio; TBR, tumor-to-blood ratio; TMR, tumor-to-muscle ratio.

led to the improvement in count utilization in ultra-low-activity imaging compared to full-activity imaging since a significantly improved fraction of effective counts was previously identified in ultra-low-activity imaging (20). These results were also supported by our experience in clinical use of the total-body scanner, with 7–15 min of acquisition time recommended for ultra-low-activity PET (32). However, the background liver SNR of L_8 was slightly lower than that of F_1 (11.31±2.11 *vs.* 13.10±2.28; P=0.003), which could be associated with the combined effect of decreased liver uptake (liver SUV_{mean}) and increased noise (liver SUV_{SD}) in L_8, as shown in *Figure 4*. Parameter optimization in image reconstruction (e.g., by reducing the iterations from 3 to 2) may improve the SNR in low-activity imaging without compromising image quality (33,34).

This study had several limitations. First, when performing model fitting of dynamic data, we did not consider the dual-blood supply of the liver. However, a single arterial input function seems more appropriate for our study, as liver malignancies are commonly supplied by the hepatic artery (35). Second, only patients with FDG-avid lesions were included for dynamic study, and only hepatic malignancies were evaluated. These might have introduced biases to the results, and thus extrapolation of these results to malignancies in other organs should be done with caution. Third, the ultra-low-activity group in the dynamic study had proportionally more cases of ICC than did the full-activity group, although not significantly so. This might have potentially affected the results, as HCC has varying degrees of ^{18}F-FDG avidity; however, this influence is likely slight because only HCC lesions with high ^{18}F-FDG uptake were included. Fourth, in the static imaging study, we excluded overweight patients [body mass index (BMI) >28 kg/m^2] to avoid the influence of overweight status on image quality since degraded image quality caused by high photon attenuation and scatter has been reported in overweight patients (36). Finally, in both the dynamic and static study, the sample sizes of our study were small for drawing a definitive conclusion. Future research with a larger sample size is needed to validate the results of our study.

Conclusions

Although the sample size was small, the results of this single-center observational study indicate that ^{18}F-FDG PET conducted with high-sensitivity total-body PET/CT scanner imaging and a 10× reduction of injection activity can achieve equal performance to that of full-activity imaging in patients with hepatic malignancies. Specifically, both dynamic imaging in quantifying the kinetic metrics of tumor and static imaging produced comparable image qualities for lesion demonstration.

Acknowledgments

Funding: This study was supported by the Shanghai Municipal Key Clinical Specialty Project (grant No. SHSLCZDZK03401), the Major Science and Technology Projects for Major New Drug Creation (grant No. 2019ZX09302001), the Shanghai Science and Technology Committee Program (grant No. 20DZ2201800), the Three-year Action Plan of Clinical Skills and Innovation of Shanghai Hospital Development Center (grant No. SHDC2020CR3079B), and the Next Generation Information Infrastructure Construction Project founded by the Shanghai Municipal Commission of Economy and Informatization (grant No. 201901014).

Footnote

Reporting Checklist: The authors have completed the STROBE reporting checklist. Available at https://qims.amegroups.com/article/view/10.21037/qims-23-719/rc

Conflicts of Interest: All authors have completed the ICMJE uniform disclosure form (available at https://qims.amegroups.com/article/view/10.21037/qims-23-719/coif). The authors have no conflicts of interest to declare.

Ethical Statement: The authors are accountable for all aspects of the work in ensuring that questions related to the accuracy or integrity of any part of the work are appropriately investigated and resolved. This retrospective study was conducted in accordance with the Declaration of Helsinki (as revised in 2013) and was approved by the Institutional Review Board of Zhongshan Hospital of Fudan University (approval No. B2019-160R). All participants provided written informed consent.

References

1. Phelps ME. Positron emission tomography provides molecular imaging of biological processes. Proc Natl Acad Sci U S A 2000;97:9226-33.
2. Badawi RD, Kohlmyer SG, Harrison RL, Vannoy SD, Lewellen TK. The effect of camera geometry on singles flux, scatter fraction and trues and randoms sensitivity for cylindrical 3D PET-a simulation study. IEEE Trans Nucl Sci 2000;47:1228-32.
3. Cherry SR. The 2006 Henry N. Wagner Lecture: Of mice and men (and positrons)--advances in PET imaging technology. J Nucl Med 2006;47:1735-45.
4. Rahmim A, Lodge MA, Karakatsanis NA, Panin VY, Zhou Y, McMillan A, Cho S, Zaidi H, Casey ME, Wahl RL. Dynamic whole-body PET imaging: principles, potentials and applications. Eur J Nucl Med Mol Imaging 2019;46:501-18.
5. Boellaard R, Delgado-Bolton R, Oyen WJ, Giammarile F, Tatsch K, Eschner W, et al. FDG PET/CT: EANM procedure guidelines for tumour imaging: version 2.0. Eur J Nucl Med Mol Imaging 2015;42:328-54.
6. Cherry SR, Badawi RD, Karp JS, Moses WW, Price P, Jones T. Total-body imaging: Transforming the role of positron emission tomography. Sci Transl Med 2017;9:eaaf6169.
7. Vandenberghe S, Moskal P, Karp JS. State of the art in total body PET. EJNMMI Phys 2020;7:35.
8. Jones T, Budinger TF. The potential for low-dose functional studies in maternal-fetal medicine using PET/MR imaging. J Nucl Med 2013;54:2016-7.
9. Badawi RD, Shi H, Hu P, Chen S, Xu T, Price PM, Ding Y, Spencer BA, Nardo L, Liu W, Bao J, Jones T, Li H, Cherry SR. First Human Imaging Studies with the EXPLORER Total-Body PET Scanner. J Nucl Med 2019;60:299-303.
10. Zhang X, Badawi RD, Cherry SR, Qi J. Theoretical study of the benefit of long axial field-of-view PET on region of interest quantification. Phys Med Biol 2018;63:135010.
11. Surti S, Karp JS. Impact of detector design on imaging performance of a long axial field-of-view, whole-body PET scanner. Phys Med Biol 2015;60:5343-58.
12. Kaplan S, Zhu YM. Full-Dose PET Image Estimation from Low-Dose PET Image Using Deep Learning: a Pilot Study. J Digit Imaging 2019;32:773-8.
13. Schaefferkoetter JD, Yan J, Sjöholm T, Townsend DW, Conti M, Tam JK, Soo RA, Tham I. Quantitative Accuracy and Lesion Detectability of Low-Dose (18)F-FDG PET for Lung Cancer Screening. J Nucl Med 2017;58:399-405.
14. Jian Y, Planeta B, Carson RE. Evaluation of bias and variance in low-count OSEM list mode reconstruction. Phys Med Biol 2015;60:15-29.
15. Schaefferkoetter JD, Yan J, Townsend DW, Conti M. Initial assessment of image quality for low-dose PET: evaluation of lesion detectability. Phys Med Biol 2015;60:5543-56.
16. Hong I, Cho S, Michel CJ, Casey ME, Schaefferkoetter JD. Complementary frame reconstruction: a low-biased dynamic PET technique for low count density data in projection space. Phys Med Biol 2014;59:5441-55.
17. Walker MD, Asselin MC, Julyan PJ, Feldmann M, Talbot PS, Jones T, Matthews JC. Bias in iterative reconstruction of low-statistics PET data: benefits of a resolution model. Phys Med Biol 2011;56:931-49.
18. Alessio AM, Kinahan PE, Manchanda V, Ghioni V, Aldape L, Parisi MT. Weight-based, low-dose pediatric whole-body PET/CT protocols. J Nucl Med 2009;50:1570-7.
19. Gühne F, Drescher R, Seifert P, Freesmeyer M. Minimal-activity PET/CT for efficacy control after SIRT (MAPECSI) - clinical implementation of a resource-saving, liver-focused protocol. Nuklearmedizin 2019;58:363-70.
20. Liu G, Hu P, Yu H, Tan H, Zhang Y, Yin H, Hu Y, Gu J, Shi H. Ultra-low-activity total-body dynamic PET imaging allows equal performance to full-activity PET imaging for investigating kinetic metrics of (18)F-FDG in healthy volunteers. Eur J Nucl Med Mol Imaging

2021;48:2373-83.
21. Tan H, Sui X, Yin H, Yu H, Gu Y, Chen S, Hu P, Mao W, Shi H. Total-body PET/CT using half-dose FDG and compared with conventional PET/CT using full-dose FDG in lung cancer. Eur J Nucl Med Mol Imaging 2021;48:1966-75.
22. Wang R, Fan Q, Tian R, Su M. Intrapatient repeatability of background (18)F-FDG uptake on PET/CT. Quant Imaging Med Surg 2021;11:4172-80.
23. Daisne JF, Duprez T, Weynand B, Lonneux M, Hamoir M, Reychler H, Grégoire V. Tumor volume in pharyngolaryngeal squamous cell carcinoma: comparison at CT, MR imaging, and FDG PET and validation with surgical specimen. Radiology 2004;233:93-100.
24. Liu G, Xu H, Hu P, Tan H, Zhang Y, Yu H, Li X, Shi H. Kinetic metrics of (18)F-FDG in normal human organs identified by systematic dynamic total-body positron emission tomography. Eur J Nucl Med Mol Imaging 2021;48:2363-72.
25. van Sluis J, Boellaard R, Somasundaram A, van Snick PH, Borra RJH, Dierckx RAJO, Stormezand GN, Glaudemans AWJM, Noordzij W. Image Quality and Semiquantitative Measurements on the Biograph Vision PET/CT System: Initial Experiences and Comparison with the Biograph mCT. J Nucl Med 2020;61:129-35.
26. Wahl RL, Jacene H, Kasamon Y, Lodge MA. From RECIST to PERCIST: Evolving Considerations for PET response criteria in solid tumors. J Nucl Med 2009;50 Suppl 1:122S-50S.
27. Juweid ME, Stroobants S, Hoekstra OS, Mottaghy FM, Dietlein M, Guermazi A, et al. Use of positron emission tomography for response assessment of lymphoma: consensus of the Imaging Subcommittee of International Harmonization Project in Lymphoma. J Clin Oncol 2007;25:571-8.
28. Xu J, Gong E, Pauly J, Zaharchuk G. 200x Low-dose PET Reconstruction using Deep Learning. arXiv:1712.04119v1, 2017. [accessed September 5, 2023]. Available online: https://doi.org/10.48550/arXiv.1712.04119
29. Zhang YQ, Hu PC, Wu RZ, Gu YS, Chen SG, Yu HJ, Wang XQ, Song J, Shi HC. The image quality, lesion detectability, and acquisition time of (18)F-FDG total-body PET/CT in oncological patients. Eur J Nucl Med Mol Imaging 2020;47:2507-15.
30. Hu P, Zhang Y, Yu H, Chen S, Tan H, Qi C, Dong Y, Wang Y, Deng Z, Shi H. Total-body (18)F-FDG PET/CT scan in oncology patients: how fast could it be? Eur J Nucl Med Mol Imaging 2021;48:2384-94.
31. Akamatsu G, Ishikawa K, Mitsumoto K, Taniguchi T, Ohya N, Baba S, Abe K, Sasaki M. Improvement in PET/CT image quality with a combination of point-spread function and time-of-flight in relation to reconstruction parameters. J Nucl Med 2012;53:1716-22.
32. Sui X, Liu G, Hu P, Chen S, Yu H, Wang Y, Shi H. Total-Body PET/Computed Tomography Highlights in Clinical Practice: Experiences from Zhongshan Hospital, Fudan University. PET Clin 2021;16:9-14.
33. Sui X, Tan H, Yu H, Xiao J, Qi C, Cao Y, Chen S, Zhang Y, Hu P, Shi H. Exploration of the total-body PET/CT reconstruction protocol with ultra-low (18)F-FDG activity over a wide range of patient body mass indices. EJNMMI Phys 2022;9:17.
34. Weber M, Jentzen W, Hofferber R, Herrmann K, Fendler WP, Rischpler C, Umutlu L, Conti M, Costa PF, Sraieb M, Kersting D. Evaluation of (18)F-FDG PET/CT images acquired with a reduced scan time duration in lymphoma patients using the digital biograph vision. BMC Cancer 2021;21:62.
35. Brix G, Ziegler SI, Bellemann ME, Doll J, Schosser R, Lucht R, Krieter H, Nosske D, Haberkorn U. Quantification of (18)FFDG uptake in the normal liver using dynamic PET: impact and modeling of the dual hepatic blood supply. J Nucl Med 2001;42:1265-73.
36. Halpern BS, Dahlbom M, Auerbach MA, Schiepers C, Fueger BJ, Weber WA, Silverman DH, Ratib O, Czernin J. Optimizing imaging protocols for overweight and obese patients: a lutetium orthosilicate PET/CT study. J Nucl Med 2005;46:603-7.

Cite this article as: Liu G, Tan H, Sui X, Qi C, Cao Y, Cai D, Hu P, Zhang Y, Shi H. One-tenth-activity total-body positron emission tomography versus full-activity imaging in patients with a complex of hepatic malignant tumors: a retrospective study. Quant Imaging Med Surg 2023;13(12):8517-8530. doi: 10.21037/qims-23-719

